APPENDIX C

A Novel Approach to Determine the Heat Transfer Coefficient in Directional Solidification Furnaces

Mohsen BANAN, Ross T. GRAY, and William R. WILCOX
Center for Crystal Growth in Space and School of Engineering
Clarkson University,
Potsdam, New York 13699, USA

Abstract

The heat transfer coefficient between a molten charge and its surroundings in a Bridgman furnace was determined using a novel approach utilizing *in-situ* temperature measurement. The ampoule containing an isothermal melt was suddenly moved from a higher temperature zone to a lower temperature zone. The temperature-time history was used in a lumped-capacity cooling model to evaluate the heat transfer coefficient between the charge and the furnace. The experimentally determined heat transfer coefficient was of the same order of magnitude as the value estimated by standard heat transfer calculations.

1 Introduction

A variety of directional solidification techniques are used for preparation of materials, especially for growth of single crystals. These include the vertical Bridgman-Stockbarger, horizontal Bridgman, gradient freeze, and zone melting techniques. It is time consuming and costly to experimentally determine the optimal thermal conditions of a furnace utilized to grow a specific material. Hence, it is desirable to employ analytical and numerical models to assist in determining the optimal thermal conditions for a specific growth system, e.g. Bridgman technique [1-6]. Such calculations are handicapped by limited knowledge of the growth environment's thermal characteristics.

The heat transfer coefficient, defined as the ratio of the heat flux to the temperature difference between the material and the furnace, is an important thermal parameter in a growth system. The heat transfer coefficient manifests itself in the heat transfer models as the Biot number hR/k, where

h is the heat transfer coefficient, R is the sample radius, and k is the thermal conductivity of the sample. The Biot number may be regarded as the ratio of the ease of heat exchange with the furnace to heat conduction through the charge.

Chang and Wilcox [1] showed that increasing the Biot number in Bridgman growth affects the position and shape of the isotherms in the furnace. The sensitivity of interface position to heater and cooler temperatures is greater for small Biot number, i.e. small ampoule diameter, ineffective heat transfer from the ampoule surface (small value of h), and high thermal conductivity of the material.

Fu and Wilcox [2] showed that decreasing the Biot numbers in the heater and cooler of a vertical Bridgman-Stockbarger system results in isotherms becoming less curved. The planar isotherms lie in the lower portion of the adiabatic zone when the heater's Biot number is larger than the cooler's Biot number. Increasing the cooler's Biot number moved the position of the planar interface toward the upper section of the adiabatic zone.

Although the heat transfer coefficient may be estimated from heat transfer principles [5,7], there are considerable uncertainties making an experimental value preferred. Here, we report a novel approach to experimentally determine the average heat transfer coefficient between the growth material and the furnace. This is accomplished by *in-situ* temperature measurement of a transiently cooled object, i.e. melt or solid contained in an ampoule. In this technique, an isothermal charge held at temperature T_o is suddenly moved to a chamber at temperature T_∞. The temperature in the charge as a function of time is measured using a thermocouple and the data obtained are used to calculate the average heat transfer coefficient between the molten charge and its surroundings using a lumped-capacity model. A GaSb charge was used to demonstrate the method. The validity of the lumped-capacity model was examined by solving the one-dimensional transient heat transfer problem between a rod and its surroundings and comparing the results of this analysis with the lumped-capacity solution. The one-dimensional transient problem takes radial temperature gradients in the rod into account.

2 Lumped-Capacity Model

The value of the heat transfer coefficient depends on the geometry of the system as well as the physical properties and temperature of the material and its environment. A simple but important

method based on a lumped-capacity solution [8] can be utilized to determine the average heat transfer coefficient between an object and its surroundings from the transient cooling of the object. This analysis assumes that the object is isothermal. This object at temperature T_o is introduced suddenly into an environment at temperature T_∞. The heat transfer coefficient is calculated from the change in temperature of the object as a function of time.

An analytical temperature-time relationship of the cooling process is obtained by equating the change in the total enthalpy of the object to the net heat flow from the object to the surroundings during time interval dt:

$$d\,[c\rho V(T - T_\infty)] = -\bar{h}A\,(T - T_\infty)\,dt, \tag{1}$$

where the symbols are defined in the table of nomenclature. Assuming c, ρ, and $\bar{h}$ to be constant, integration of equation (1) from T_o to T over time t gives:

$$\ln\,(T - T_\infty) = \ln\,(T_o - T_\infty) - \frac{\bar{h}At}{c\rho V}. \tag{2}$$

Transforming the above equation into a non-dimensional form yields:

$$\ln\theta = (-2Bi)\tau, \tag{3}$$

where Bi=hR/k, $\theta = (T\text{-}T_\infty)/(T_o\text{-}T_\infty)$, and $\tau = \alpha t/R^2$. Thus, the Biot number is found from the slope of a $\ln\theta$ versus τ plot and the heat transfer coefficient is given by:

$$\bar{h} = \frac{Bi\ k}{R}. \tag{4}$$

In our experiments, the object consisted of a molten GaSb charge contained in a quartz ampoule (discussed in detail in the experimental section). The environment was a vertical Bridgman-Stockbarger furnace. The ampoule wall added a resistance to the heat transfer between the charge and the furnace. To include the effect of such resistance on the heat transfer coefficient, some modifications of the thermophysical properties in equations (1-4) were necessary. (A similar approach was undertaken by Naumann [5].) A mass weighted effective thermal conductivity and thermal diffusivity are defined as follows:

$$k_{eff} = \frac{\rho_c V_c k_c + \rho_{qa} V_{qa} k_{qa}}{\rho_c V_c + \rho_{qa} V_{qa}}, \tag{5}$$

$$\alpha_{eff} = \frac{k_{eff}}{\rho_{avg} c_{eff}} = \frac{(\rho_c V_c k_c + \rho_{qa} V_{qa} k_{qa})(V_c + V_{qa})}{(\rho_c V_c c_c + \rho_{qa} V_{qa} c_{qa})(\rho_c V_c + \rho_{qa} V_{qa})}, \tag{6}$$

where all parameters are defined in the table of nomenclature. The effective heat transfer coefficient then becomes:

$$\bar{h}_{eff} = \frac{Bi_{eff} k_{eff}}{R_a}, \tag{7}$$

where R_a is the outer radius of the ampoule and Bi_{eff} is found from the slope of the $\ln\theta$ versus $\tau_{eff} = \alpha_{eff} t/R_a^2$ plot.

3 Validity of the Lumped-Capacity Model

In order to determine the validity of the lumped-capacity model for different ranges of the Biot number, a similar model was solved which takes radial temperature gradients in the sample into account. This model assumes that the heat flow is axisymmetric, the temperature in the rod is uniform in the axial direction, and the density, specific heat, and thermal conductivity of the rod are independent of temperature. It is valid for any values of the Biot number. The solution to this problem for the dimensionless temperature at the centerline of the rod is given in Carslaw and Jaeger [10] as:

$$\Theta = \frac{T - T_\infty}{T_o - T_\infty} = 2\sum_{n=1}^{\infty} \frac{Bi}{J_o(\Gamma_n)(\Gamma_n^2 + Bi^2)} \exp\left(-\Gamma_n^2 \tau\right), \tag{8}$$

where the eigenvalues Γ_n are roots of the equation:

$$\Gamma_n J_1(\Gamma_n) = Bi\, J_o(\Gamma_n), \tag{9}$$

and J_o and J_1 are Bessel functions of order zero and one, respectively. For the range of Biot numbers studied, ten terms of the infinite series were determined to yield an accuracy of more than 5 significant digits in θ.

When the series in equation (8) is truncated after the first term, the following equation is obtained:

$$\ln\Theta_1 = \ln\left\{\frac{2Bi}{J_o(\Gamma_1)\,(\Gamma_1^2 + Bi^2)}\right\} - \Gamma_1^2 \tau. \tag{10}$$

In order to determine when the series could be truncated after the first term, the error in truncation had to be determined as a function of dimensionless time τ and Biot number. The relative truncation error was defined to be $(\theta_1 - \theta)/\theta$, where θ is the exact solution which was taken as the value of θ when the series was truncated after ten terms. The dimensionless time τ_{crit} past which the truncation error is less than 0.01 was plotted in Figure 1 for values of the Biot number between

0 and 0.9. For values of the Biot number between about 0.05 and 0.9, the critical dimensionless time is given by the 5^{th} order polynomial fit:

$$\tau_{crit} = 3.02\ \mathrm{Bi}^5 - 8.54\ \mathrm{Bi}^4 + 9.32\ \mathrm{Bi}^3 - 5.03\ \mathrm{Bi}^2 + 1.48\ \mathrm{Bi} - 0.0302. \tag{11}$$

This means that equation (10) is valid for all Biot numbers as long as the dimensionless time is greater than τ_{crit}. A plot of $\ln\theta$ versus τ should be linear after time τ_{crit}.

If a linear regression analysis is carried out on experimental data at dimensionless times greater than τ_{crit}, Γ_1 is given by the square root of the negative of the slope. This value can then be used to calculate the Biot number by two different methods. A value for the Biot number can be found by solving equation (9). Also, the Biot number can be calculated from the intercept b_o by finding the root of the equation:

$$\mathrm{f(Bi)} = e^{b_o} - \frac{2\mathrm{Bi}}{J_o(\Gamma_1)\,(\Gamma_1^2 + \mathrm{Bi}^2)} = 0. \tag{12}$$

The value of the Biot number calculated from the intercept is much more susceptible to experimental error. When doing a linear regression analysis, the value of the slope is much more statistically significant than the value of the intercept. This is because the intercept is at the edge of the experimental data. Also, the Biot number is much more sensitive to small errors in the intercept than in the slope. Figure 2 shows the dependence of the Biot number on the intercept b_o and slope m of equation (10). The solid line is a linear fit of the Biot number versus the intercept, and is given by:

$$\mathrm{Bi} = 4.24\ b_o. \tag{13}$$

The dashed line is a linear fit of the Biot number versus the negative of the slope, and is given by:

$$\mathrm{Bi} = 0.503\ (-\mathrm{m}). \tag{14}$$

Thus, the Biot number is about eight times more sensitive to experimental errors in the intercept than the slope. Another uncertainty when calculating the Biot number from the intercept is that the experimentally determined value of the slope must be used in equation (12) to find the intercept. This is an additional source of error.

Equation (10) is similar to the lumped-capacity solution, except that the intercept is not zero and the slope is $-\Gamma_1^2$ as compared to $-2\cdot\mathrm{Bi}$ from the lumped-capacity model. The validity of the lumped-capacity solution can be assessed by calculating the relative error caused by assuming the

Biot number equals the negative of the slope of a $\ln\theta$ versus τ plot divided by two. The relative error can be defined as $(\text{Bi}-\Gamma_1^2/2)/\text{Bi}$, where Bi is the actual Biot number and Γ_1 is calculated from equation (9). The relative error is plotted in Figure 3 as a function of Biot number and is given by the 2^{nd} order polynomial fit:

$$\text{Relative Error} = -0.0373\ \text{Bi}^2 + 0.248\ \text{Bi}, \tag{15}$$

for Biot numbers between 0 and 0.9. The relative error is almost a linear function of Biot number in this region.

This analysis suggests that care must be taken when applying the lumped-capacity model to experimental data. A linear regression analysis should only be done for values of $\tau > \tau_{crit}$. When the Biot number is large, most of the temperature change could occur before τ_{crit} and the error in assuming the slope equals -2·Bi becomes large. Furthermore, the experimental errors in temperature measurement become large when T approaches T_∞. This is best demonstrated by example. Let us consider the case when $T_o = 800°C$, $T_\infty = 700°C$, and the error in measurement of the temperature is 1°C. If the actual temperature is 750°C, the error in the resulting value of $\ln\theta$ is only 3%. However, when the actual temperature is 701°C, the error is 15%.

Another important point when applying the lumped-capacity model is that the straight line should not be forced through the origin. A two-parameter regression analysis should be performed, as suggested by equation (10).

4 Experimental

The lumped-capacity technique was demonstrated using an ampoule and thermocouple arrangement containing molten GaSb situated in the heater of a Bridgman-Stockbarger furnace at temperature T_o. The ampoule was moved suddenly to a region of different temperature T_∞. The temperature versus time data were collected as the melt equilibrated to the new temperature and the lumped-capacity model was used to determine the heat transfer coefficient between the ampoule and furnace.

A schematic diagram of the experimental apparatus is shown in Figure 4. It consisted of a 3-zone vertical Bridgman-Stockbarger furnace. The heating zones of the furnace were made of Kanthal heating elements embedded in Fibrothal insulation. The 5 cm long adiabatic zone was

fabricated from zirconia insulation. The zones' temperatures were controlled to withing $\pm 1°C$ using digital PID temperature controllers and SCRs. Quartz tubing was used as a liner in the furnace. Two type K thermocouples, inserted halfway into the heaters between the furnace wall and the liner, were used for control. Both ends of the furnace were plugged to eliminate the chimney effect.

The 0.9 cm ID and 1.1 cm OD quartz growth ampoule, shown in Figure 5, was loaded with a 7 cm long GaSb charge, compounded from six-9s purity Ga and Sb in a rocking furnace for 5 hours at 820°C. The temperature in the melt was measured using a 0.041 cm diameter grounded K-type thermocouple with a 310 stainless steel sheath and MgO as insulation (made by General Measurements). The tip of the thermocouple was positioned 3 cm into the ampoule at the center of the charge.

The molten charge was allowed to reach thermal equilibrium with the surroundings prior to each experiment. For experiments H1 and H2, the loaded ampoule was positioned in the lower zone, set at 890°C. The upper zone's setting was at 800°C. After the thermocouple reading became stable, the ampoule was suddenly moved to the upper zone and held firmly. Meanwhile, the thermocouple output was collected using a data acquisition system. In experiment H3, the upper and lower zones were set at 870°C and 780°C, respectively. The ampoule in experiment H3 was initially positioned in the upper zone. After the temperature became stable, the ampoule was suddenly moved downward into the lower zone and held in the central region of this zone. The temperature was recorded versus time using a data acquisition system.

5 Results

5.1 Experimental Determination of Heat Transfer Coefficients

Figures 6 and 7 show the actual thermocouple readings collected from the molten GaSb during experiments H1, H2, and H3. The logarithm of the dimensionless temperature θ was plotted versus dimensionless time τ_{eff} in Figures 8-10. A linear regression analysis using NCSS Statistical Software was performed to determine the slopes and intercepts of these plots.

Figure 7 depicts the experimental data and the resulting linear fit for experiment H1, where the GaSb charge was raised from the lower zone at 890°C to the upper zone at 800°C. The value of T_o was 871.3°C and T_∞ was 792.3°C. The linear regression analysis was performed on the data

for τ_{eff} between 0.1 and 18. There are two reasons that these limits for τ_{eff} were chosen. The value of τ_{crit}, beyond which the relationship between $\ln\theta$ and τ_{eff} is linear, is less than 0.1. Also, the experimental data tend to bend upward beyond $\tau_{eff} = 18$. The reason for this is the magnification of experimental error at small values of θ. (Both of these explanations are discussed fully in section 3.) The resulting linear fit is $\theta = (-0.142 \pm 0.0006)\tau + (0.0697 \pm 0.0059)$. The uncertainty values are 95% confidence limits on the slope and intercept, which can be transformed into 95% confidence limits on the Biot number. The lumped-capacity solution leads to a Biot number of 0.0712 ± 0.0003 determined from the slope. The two values of the Biot number determined using the model accounting for radial temperature gradients are 0.0725 ± 0.0003 from equations (9 & 10) and 0.0767 ± 0.0008 from equations (10 & 12).

The same analysis as above was performed for experiment H2, which was a repeat of experiment H1 described above. However, T_o was 876.3°C and T_∞ was 793.6°C in this experiment. The reason for the difference in these values from those of experiment H1 was probably a difference in initial and final positions of the charge for the two experiments. The linear regression analysis was performed on the data for τ_{eff} between 0.1 and 20 and the result is shown in Figure 8. The linear fit is $\theta = (-0.138 \pm 0.0004)\tau + (0.0407 \pm 0.0042)$. The lumped-capacity solution leads to a Biot number of 0.0689 ± 0.0002 determined from the slope. The two values of the Biot number determined using the model accounting for radial temperature gradients are 0.0701 ± 0.0002 from equations (9 & 10) and 0.0719 ± 0.0005 from equations (10 & 12).

The analysis was performed for experiment H3, where the GaSb charge was lowered from the upper zone at 870°C to the lower zone at 780°C. The value of T_o was 854.5°C and T_∞ was 762.5°C. The linear regression analysis was performed on the data for τ_{eff} between 0.1 and 15 and the result is shown in Figure 10. The linear fit is $\theta = (-0.171 \pm 0.0008)\tau + (0.0522 \pm 0.0073)$. The lumped-capacity solution leads to a Biot number of 0.0855 ± 0.0004 determined from the slope. The two values of the Biot number determined using the model accounting for radial temperature gradients are 0.0873 ± 0.0004 from equations (9 & 10) and 0.0903 ± 0.0012 from equations (10 & 12).

The heat transfer coefficients obtained for experiments H1, H2, and H3 are presented in Table 1. There are three different values for each experiment. One is from the lumped-capacity model and two are from the model which accounts for radial temperature gradients.

5.2 Theoretical Estimation of Heat Transfer Coefficients

The heat transfer coefficient between the ampoule wall and the furnace could also be estimated by a simple heat transfer formulation. The heat transfer coefficient is derived by summing the heat transfer by radiation and conduction through the air gap between the ampoule and the furnace wall in a concentric cylindrical system and equating it to the heat flux Q through the ampoule containing the growth materials:

$$Q = \bar{h}(T_h - T_a) = \sigma\epsilon F(T_h^4 - T_a^4) + \frac{k_{air}(T_h - T_a)}{R_a \ln(R_f/R_a)} \tag{16}$$

The heat transfer coefficient determined from the above equation is:

$$\bar{h} = \sigma\epsilon F(T_h^2 + T_a^2)(T_h + T_a) + \frac{k_{air}}{R_a \ln \frac{R_f}{R_a}}. \tag{17}$$

The contribution of natural convection between the ampoule and the furnace was determined by computing the Grashof number in the air gap between the ampoule and the quartz liner:

$$Gr = \frac{g\beta_{air}(T_h - T_a)(R_l - R_a)^3 {\rho_{air}}^2}{\mu^2}. \tag{18}$$

We estimated the Grashof number for our experiments to be 246. Since this is less than 1000 [11], we concluded that the contribution of natural convection to the heat transfer was not significant. Therefore, the convective heat transfer term was not included in equation (16).

The view factor F = 0.9 was approximated using the view factor for finite-length concentric cylinders (i.e. furnace-ampoule) [13]. The ampoule temperature T_a was assumed to be the same as the temperature of the molten charge, since the ampoule wall was relatively small compared to the charge diameter. The steady-state temperature reading in the charge T_∞ and the temperature of the control thermocouple were used for T_a and T_h, respectively. The values of T_a = 792.5°C and T_h = 800°C for experiments H1 and H2, and T_a=762°C and T_h=780°C for experiment H3 were used in calculation of the heat transfer coefficients.

Using equation (17), the values of h calculated for experiments H1, H2, and H3 were 0.0220 (W/cm^2·K), 0.0220 (W/cm^2·K), and 0.0189 (W/cm^2·K), respectively. The estimated heat transfer coefficients are compared with the experimentally determined values in Table 1.

6 Discussion

Figure 11 depicts the comparison between the Biot numbers calculated from the lumped-capacity model ($Bi = -m/2$) and from the model including radial temperature gradients ($\Gamma_1 = \sqrt{-m}$, $Bi = \Gamma_1 J_1(\Gamma_1)/J_o(\Gamma_1)$). The horizontal and vertical lines in the figure represent 95% confidence limits on the values of the Biot number. The three data points would fall along the solid diagonal line if the results from the lumped-capacity model agreed exactly with the theory which considers radial temperature gradients in the charge. The dotted line represents the calculated relative error between the two models and is given by equation (15).

The Biot numbers calculated from the model accounting for radial temperature gradients were greater than those calculated from the lumped-capacity model. The fact that the three data points fall on the dotted line proves the relationship between the lumped-capacity Biot number and the radial temperature gradient Biot number is satisfied exactly. If the Biot number is determined using the simple lumped-capacity model, the correct Biot number can be calculated by finding the root of the rearranged form of equation (15):

$$f(Bi) = 0.0373\ Bi^3 - 0.248\ Bi^2 + Bi - Bi_L = 0, \tag{19}$$

for values of the Biot number between 0 and 0.9, where Bi_L is the Biot number calculated using the lumped-capacity model.

In theory, the value of the Biot number obtained from the slope and equation (9) should be the same as the value obtained using the intercept. The solution to the problem which accounted for radial temperature gradients was for a charge made of a single material, while the charge in our experiments consisted of a molten semiconductor contained in a quartz ampoule. When radial temperature gradients were considered, the procedure of using mass weighted thermal properties probably led to underestimation of the radial temperature gradients present. The ampoule, which caused a discontinuity in the radial temperature profile, acted as an additional barrier to heat transfer that could not be properly accounted for by adjusting the physical properties. The difference between the values of the Biot number obtained from the slope using equation (9) and from the intercept represents a failure of the exact model.

Experiments H1 and H2 were almost identical, yet the Biot numbers calculated from each differ by about 4%. This difference could have been caused by a change in the position of the

charge within the furnace. The length of the heated zones were 15 cm, not overly long compared to the charge length of 7 cm. It is possible that one or both experiments were influenced by the charge being positioned in a region where the temperature changed with height in the furnace. This would cause axial temperature gradients in the melt which would violate the assumptions of the models used. However, differences in Biot numbers less than 10% are not significant when considering the fact that heat transfer coefficients depend continuously on position in a crystal growth furnace, and this technique is being used to get an overall value for the heat transfer coefficient in a zone.

The Biot number calculated from experiment H3 was about 20% higher than those calculated from experiments H1 and H2. Experiments H1 and H2 measured the heat transfer coefficient in the upper zone, while experiment H3 measured that in the lower zone. The difference in heat transfer characteristics between the upper and lower zones was unexpected. These zones are constructed identically. The temperature rolls off at the bottom of the lower zone. It is possible that this temperature gradient led to axial heat transfer which increased the heat transfer coefficient.

It is also possible that natural convection was present in the liquid during the experiments. However, the effect of natural convection would not be expected to be large in a low Prandtl number fluid like a semiconductor melt.

The values of the heat transfer coefficient calculated experimentally differ by only 15% from simple theoretical estimations. This difference is quite small and could be due to inaccuracies in the values of emissivity and view factor.

7 Conclusions

A novel and practical approach was developed to determine the average heat transfer coefficient between a charge and directional solidification furnace. An ampoule containing molten GaSb and a thermocouple was suddenly moved from a high temperature region to a lower temperature region. The temperature decay versus time was recorded and used in a lumped-capacity model to determine the effective Biot number between the charge and furnace. The validity of the lumped-capacity method was assessed using a model which accounted for radial temperature gradients in the charge.

It was determined that the lumped-capacity model is accurate within a relative error given by equation (15) for Biot numbers between 0 and 0.9. However, this is only if the linear regression

analysis on the $\ln\theta$ versus τ plot is carried out for values of time greater than a critical dimensionless time. This dimensionless time τ_{crit} is given by equation (11) for Biot numbers between 0.05 and 0.9. The straight line fit should not be forced through the origin, since the theory which accounts for radial temperature gradients predicts a slope and a non-zero intercept. For values of τ greater than τ_{crit}, the Biot number can be determined exactly by obtaining Γ_1 from the slope of a $\ln\theta$ versus τ plot. This value can then be used to calculate the Biot number from equation (9) or used in conjunction with the intercept of the $\ln\theta$ versus τ plot to find the Biot number from equation (12). However, the value of the Biot number determined using the intercept is much more susceptible to experimental errors.

The difference between the experimentally determined Biot numbers calculated from the lumped-capacity model and the model accounting for radial temperature gradients was exactly as predicted by theory. If the Biot number is determined using the simple lumped-capacity model, the correct Biot number can be calculated by finding the root of equation (19) for values of the Biot number between 0 and 0.9. However, with the computing power and canned software available today, it might be easier to find the Biot number directly from equations (9 & 10). The Fortran functions DBSJ0 and DBSJ1 from the IMSL Library [19] were used by the authors to calculate the Bessel functions J_o and J_1, respectively.

The heat transfer coefficient between the ampoule wall and the furnace was estimated by a simple heat transfer formulation accounting for conduction and radiation across the air gap between the furnace and ampoule. Remarkably, the results differ by only 15% from the values calculated by the lumped-capacity method.

Acknowledgement

This work was supported by NASA under contracts NAG8-541 and NGT-50310.

Nomenclature

- A : Surface area of the charge (17.28 cm^2).
- b_o : Intercept of equation (10).
- Bi : Biot number $\frac{\bar{h}R}{k}$.
- Bi_{eff} : Effective Biot number between the charge+ampoule and furnace $\frac{\bar{h}_{eff}R_a}{k_{eff}}$.
- Bi_L : Biot number calculated by the lumped-capacity method.
- c_c : Specific heat capacity of the molten GaSb charge calculated using thermal conductivity, thermal diffusivity, and density data (for GaSb 0.328 J/g·K).
- c_{eff} : Mass weighted average effective specific heat capacity of charge+ampoule combination. $c_{eff} = \frac{\rho_c V_c c_c + \rho_{qa} V_{qa} c_{qa}}{\rho_c V_c + \rho_{qa} V_{qa}}$ (0.479 J/g·K for present experiments).
- c_{qa} : Specific heat capacity of ampoule (c_{qa}=1.19 J/g·K at 1075 K for fused silica [12]).
- F : View factor from furnace wall to the ampoule (0.9 for present configuration).
- g : Gravitational acceleration (980 cm/s^2).
- $\bar{h}$: Average heat transfer coefficient between the growth material and the furnace ($W/cm^2 \cdot K$).
- $\bar{h}_{eff}$: Effective average heat transfer coefficient between the charge+ampoule and the furnace ($W/cm^2 \cdot K$).
- J_n : Bessel function of order n.
- k_c : Thermal conductivity of the charge (0.171 W/cm·K for molten GaSb [13]).
- k_{eff} : Mass weighted effective thermal conductivity of charge+ampoule $k_{eff} = (\frac{\rho_c V_c k_c + \rho_{qa} V_{qa} k_{qa}}{\rho_c V_c + \rho_{qa} V_{qa}})$. (0.146 W/cm·K).
- k_{air} : Thermal conductivity of air (5.2×10^{-4} W/cm·K at 1100 K [14]).
- k_{qa} : Thermal conductivity of ampoule wall (2.42×10^{-5} T + 4.48×10^{-3} W/cm·K for fused silica [15], k_{qa} = 0.0308 W/cm·K at T=1075 K).
- L : Length of the charge (7 cm).
- m : Slope of linear equation.
- R_a : Outside radius of ampoule (0.55 cm).
- R_c : The charge radius (0.45 cm).
- R_f : Inside radius of furnace (3.81 cm).
- R_l : Radius of the furnace liner (1.0 cm).
- t : Time (s).
- T : Temperature at time t (°C).

T_∞ : Steady state temperature of the melt (°C).

T_f : Furnace temperature (°C).

T_a : Ampoule temperature (°C).

V_{qa} : Volume of the section of ampoule containing the charge;
$V_{qa} = \pi L(R_a^2 - R_c^2)$ (2.2 cm^3).

V_c : Volume of the charge (4.46 cm^3).

α_c : Thermal diffusivity of charge (0.087 cm^2/s for molten GaSb [13]).

α_{eff} : Effective thermal diffusivity of charge+ampoule (0.0628 cm^2/s).

β_{air} : Thermal expansion coefficient of air (0.00367 1/K [15]).

ϵ : Emissivity of the furnace (for Kanthal [18] $\epsilon = 0.75$).

θ : Dimensionless temperature $((T - T_\infty)/(T_o - T_\infty))$.

μ : Viscosity of air (1.84×10^{-4} g/cm·s [15]).

ρ_{air} : Density of air (1.19×10^{-3} (g/cm^3 [15]).

ρ_{av} : Average density of charge+ampoule, $\rho_{av} = \frac{\rho_c V_c + \rho_{qa} V_{qa}}{V_c + V_{qa}}$ (4.85 g/cm^3).

ρ_c : Density of charge (5.98 g/cm^3 for molten GaSb at 800°C [17]).

ρ_{qa} : Density of ampoule wall, ($2.28\times10^{-4}T + 2.273$ g/cm^3 for fused silica [16]
$\rho_{qa} = 2.586$ g/cm^3 at 1075 K).

σ : Stephan-Boltzman constant (5.67×10^{-12} $W/cm^2\cdot K^4$).

τ : Dimensionless time ($\frac{\alpha t}{R^2}$).

τ_{eff} : Effective dimensionless time ($\frac{\alpha_{eff} t}{R_a^2}$).

Γ_n : n^{th} eigenvalue.

References

[1] C.E. Chang and W.R. Wilcox, *J. Crystal Growth* **21** (1974) 135.

[2] T.W. Fu and W.R. Wilcox, *J. Crystal Growth* **48** (1980) 416.

[3] F.M. Carlson, A.L. Fripp, and R.K. Crouch, *J. Crystal Growth* **68** (1984) 747.

[4] C.J. Chang and R.A. Brown, *J. Crystal Growth* **63** (1983) 343.

[5] R.J. Naumann, *J. Crystal Growth* **58** (1982) 554.

[6] P.C. Sukanek, *J. Crystal Growth* **58** (1982) 208.

[7] T.W. Fu, Ph.D. Thesis, Clarkson University (1981).

[8] J.H. Luhard, **A Heat Transfer Textbook** (Prentice Hall, New Jersey 1981).

[9] M.N. Ozisik, **Heat Transfer; A Basic Approach** (McGraw-Hill, New York 1985).

[10] H.S. Carslaw and J.C. Jaeger, **Conduction of Heat in Solids**, 2^{nd} Edition (Oxford Press, London 1959).

[11] W.H. McAdams, **Heat Transmission**, 3^{rd} Edition (McGraw-Hill, New York 1954).

[12] E.B. Shand, **Glass Engineering Handbook**, 2^{nd} Edition (McGraw-Hill, New York 1958).

[13] A.S. Jordan, *J. Crystal Growth* **71** (1985) 551.

[14] R.C. Weast, **Handbook of Chemistry and Physics**, (CRC Press 1986).

[15] Y.S. Touloukian, R.W. Powell, C.Y. Ho, and P.G. Klemens, **Thermophysical Properties of Matter, Vol. 2 Thermal Conductivities**, (IFI/Plenum Data Corp., New York 1970).

[16] Y.S. Touloukian, R.K. Kirby, R.E. Taylor, and T.Y.R. Lee, **Thermophysical Properties of Matter, Vol. 13 Thermal Expansion**, (IFI/Plenum Data Corp, New York 1973).

[17] V.M. Glazov, S.N. Chizherskaya, and N.N. Glagoleva, **Liquid Semiconductors**, (Plenum Press, New York 1969).

[18] Kanthal Corporation, Bethel, CT.

[19] IMSL Library, 8^{th} Edition (IMSL, Inc., Houston 1980).

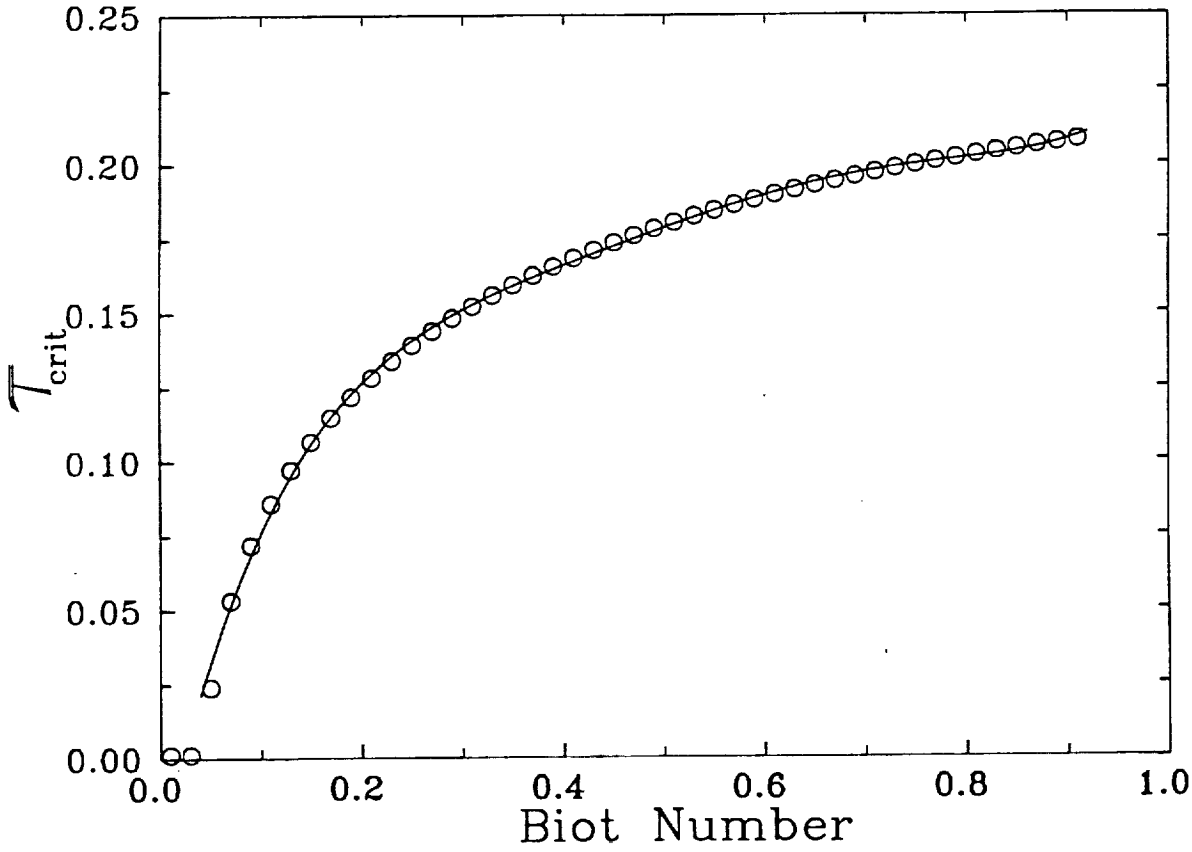

Figure 1. The dimensionless time τ_{crit} versus Biot number past which the error in θ caused by truncation of equation (8) after the first term is less than 0.01. The line represents the 5^{th} order polynomial fit given by equation (11).

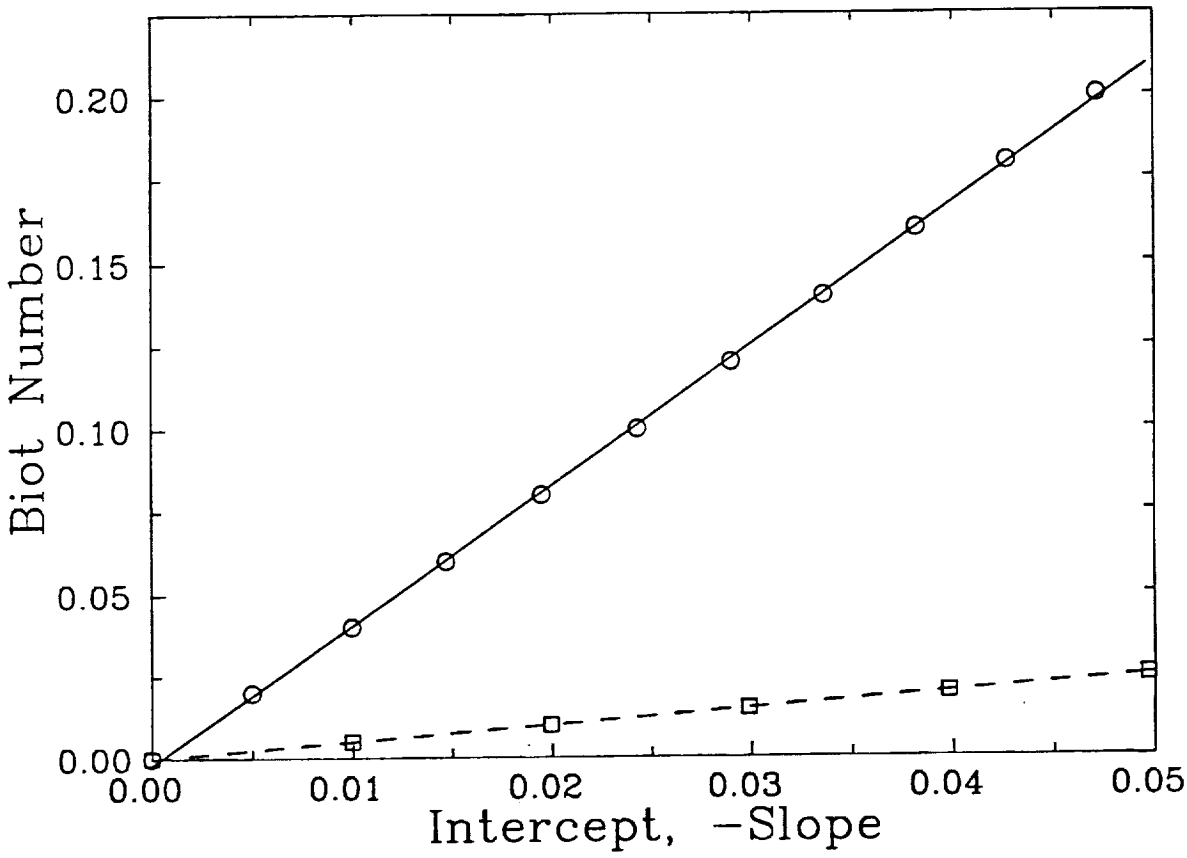

Figure 2. The dependence of the Biot number on the intercept b_o and slope m of equation (10). The solid line is the linear fit of the Biot number versus the intercept given by equation (13) and the dashed line is the linear fit of the Biot number versus the negative of the slope given by equation (14).

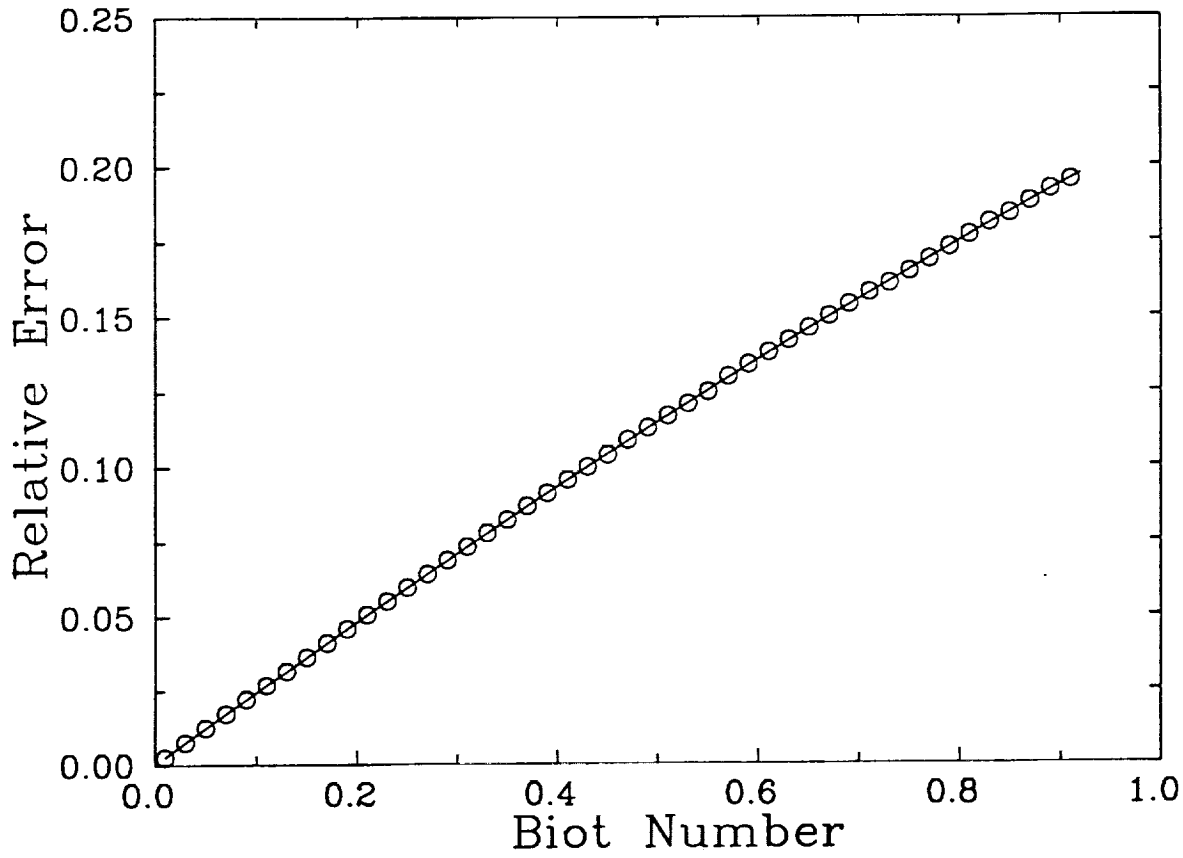

Figure 3. Relative error caused by assuming the Biot number equals -0.5 times the slope of a $\ln\theta$ versus τ plot. The line represents the 2^{nd} order polynomial fit given by equation (15).

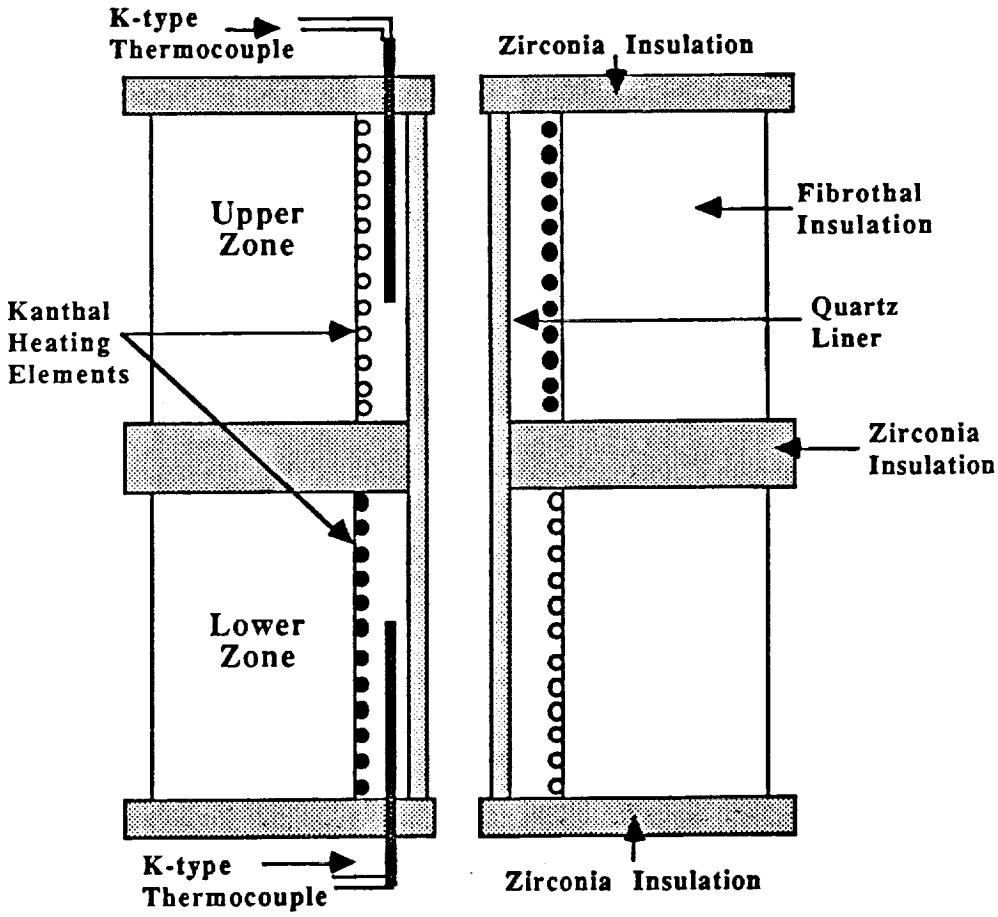

Figure 4. Schematic diagram of vertical Bridgman-Stockbarger furnace.

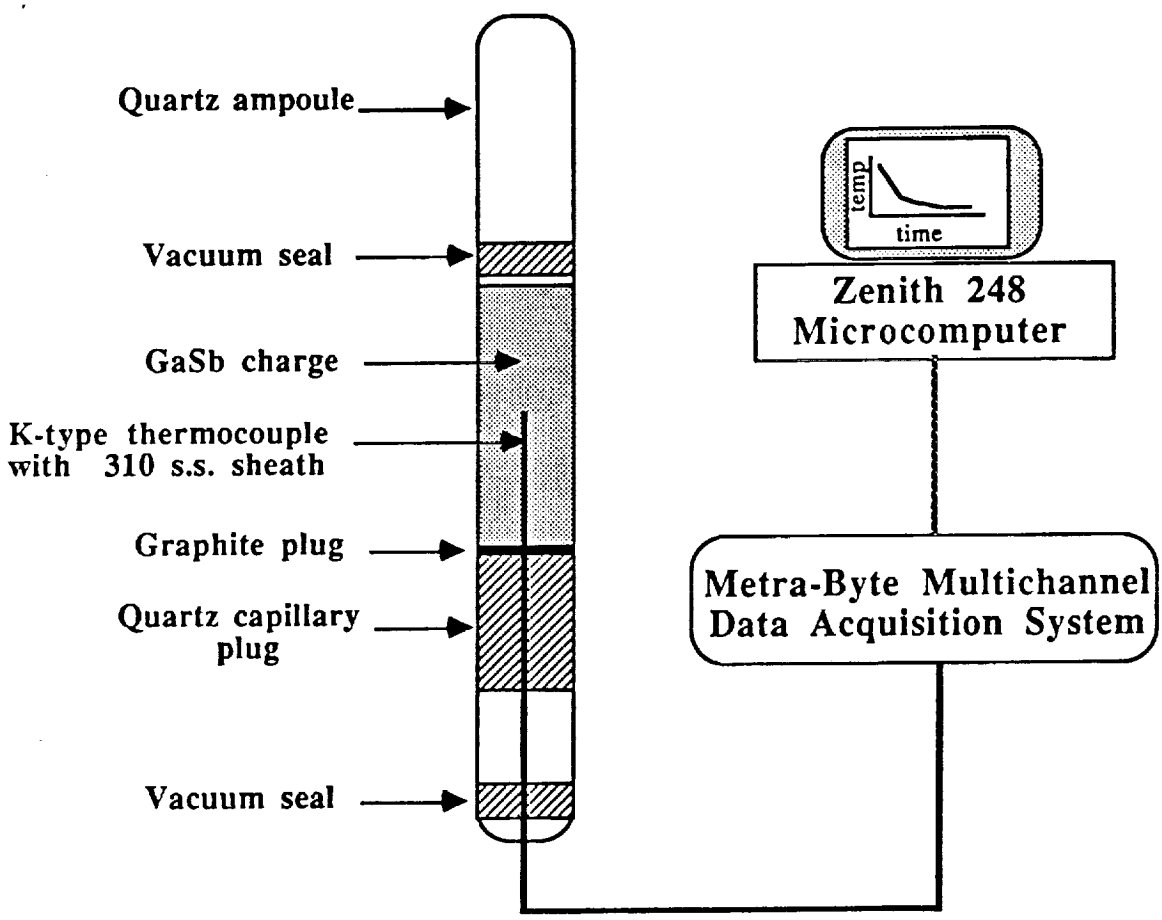

Figure 5. Schematic diagram of ampoule and thermocouple arrangement with data acquisition system for *in-situ* temperature measurements.

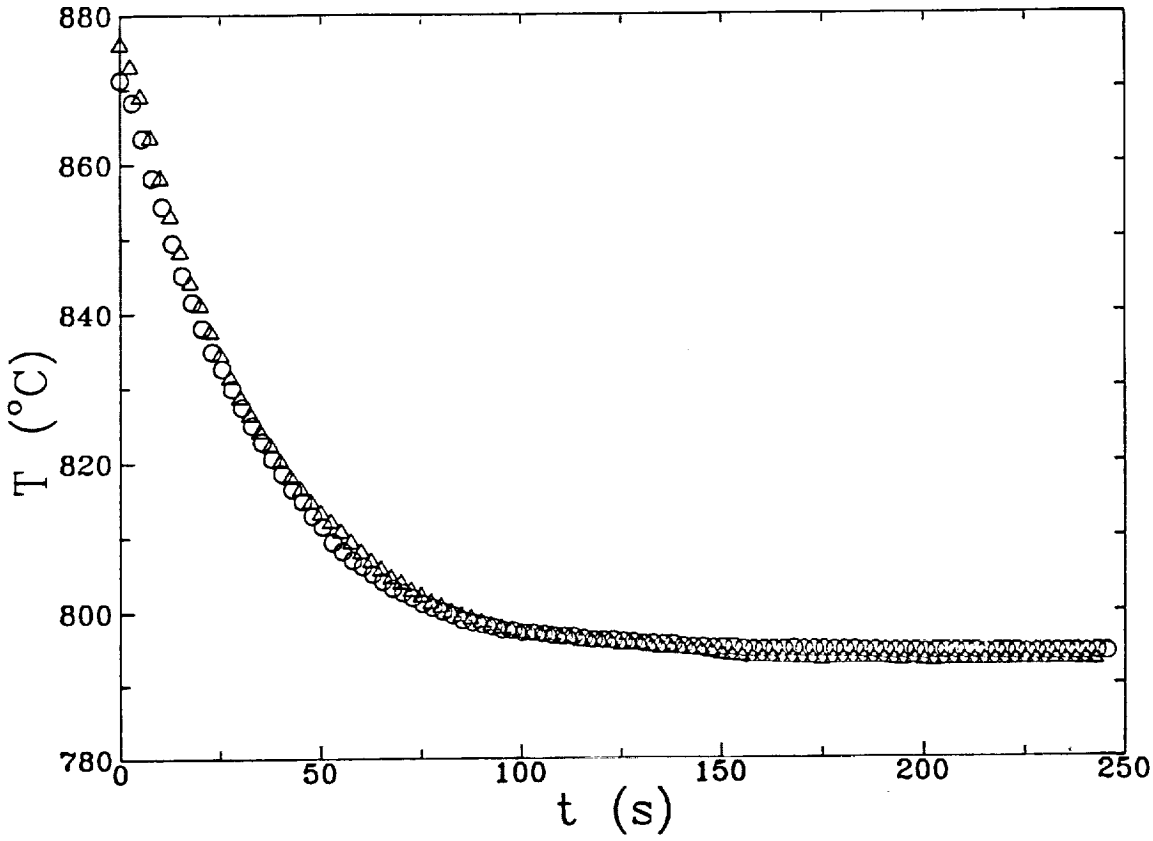

Figure 6. Thermocouple readings in molten GaSb. The circles and triangles represent the data of experiments H1 and H2, respectively.

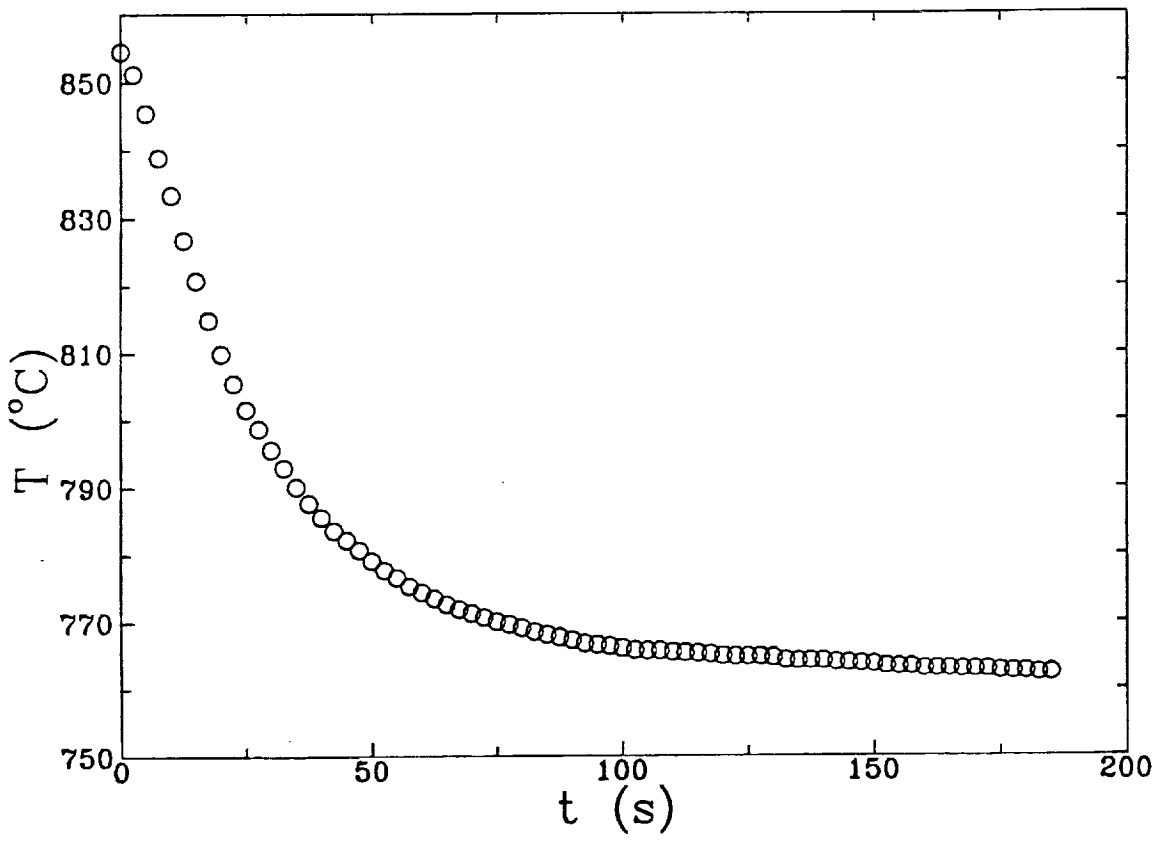

Figure 7. Thermocouple readings in molten GaSb for experiment H3.

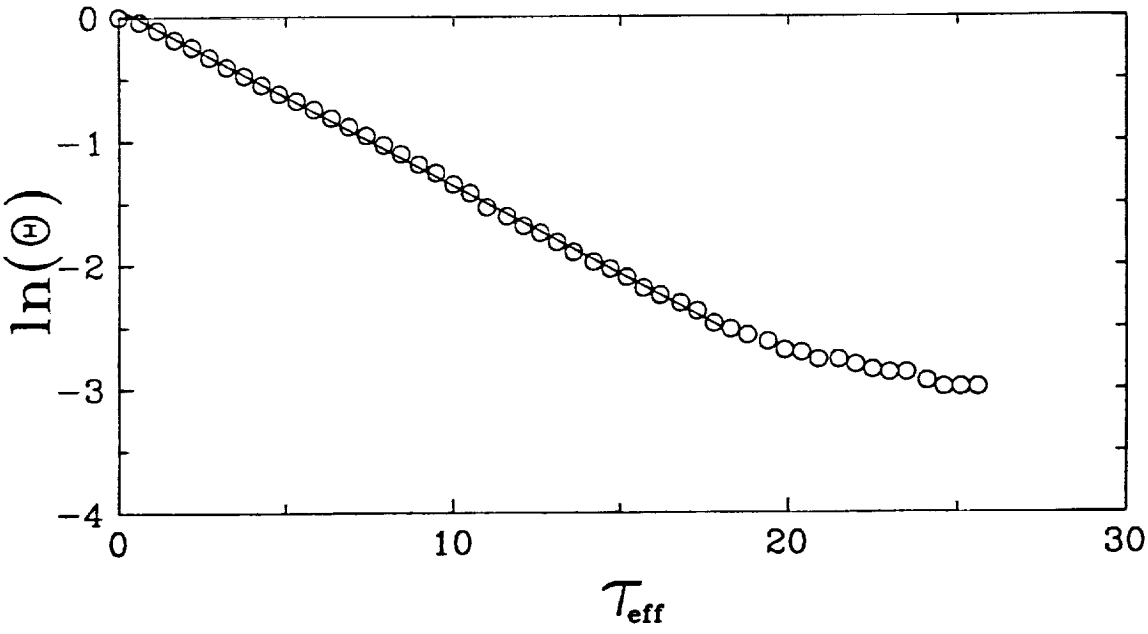

Figure 8. Experimental data and the resulting linear fit ($R^2 = 0.9993$) for experiment H1.

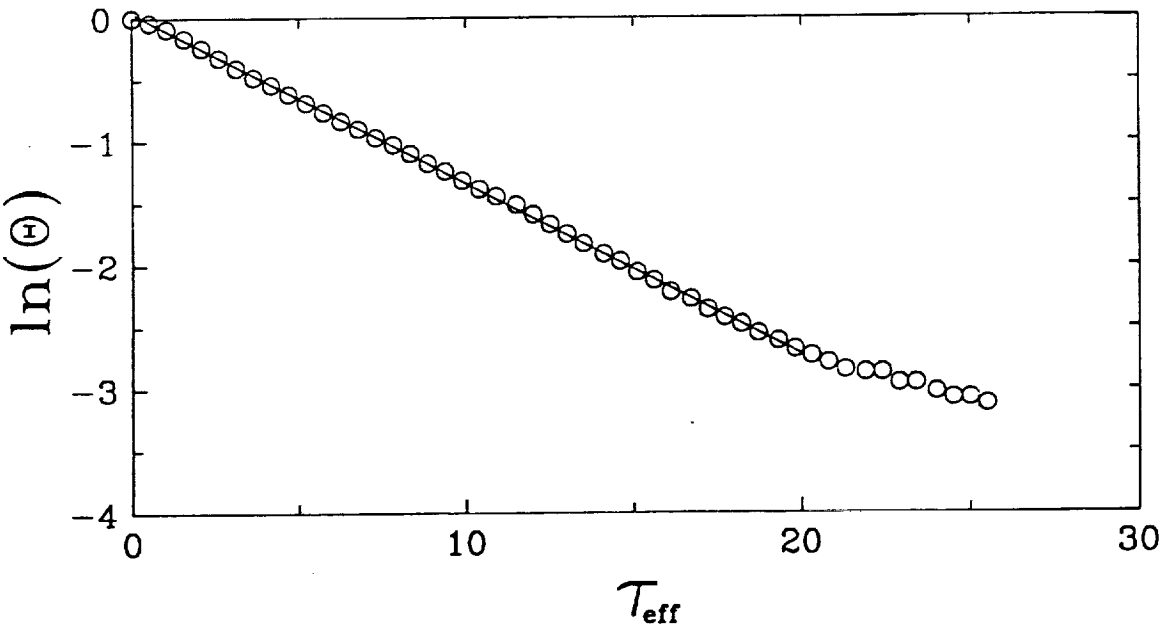

Figure 9. Experimental data and the resulting linear fit ($R^2 = 0.9997$) for experiment H2.

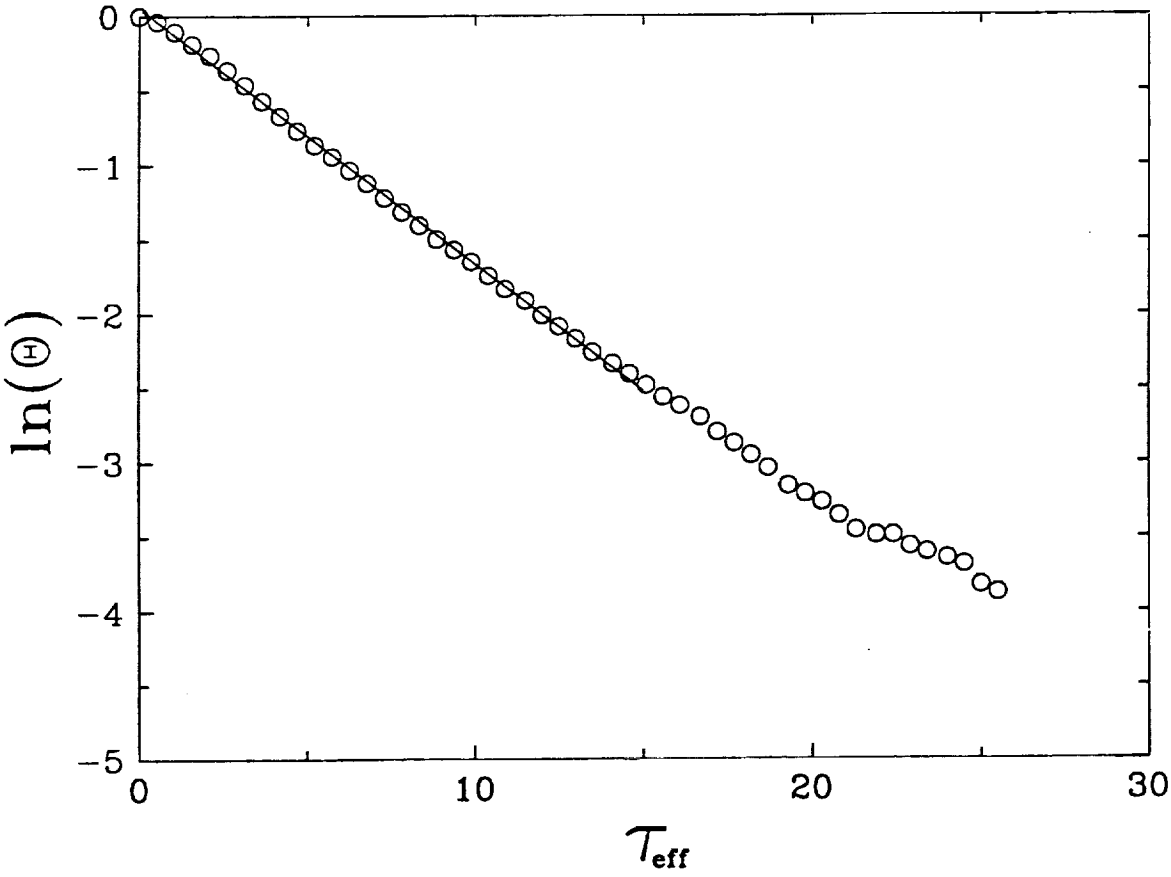

Figure 10. Experimental data and the resulting linear fit ($R^2 = 0.9991$) for experiment H3.

Experiment	h ($W/cm^2 \cdot K$)			
	Lumped-Capacity Model	Radial Model		Theoretical Estimation
		Equations (9 & 10)	Equations (10 & 12)	
H1	0.0189	0.0193	0.0204	0.0220
H2	0.0183	0.0186	0.0191	0.0220
H3	0.0227	0.0232	0.0240	0.0189

Table 1. Comparison of the experimentally determined and theoretically estimated values of the heat transfer coefficient for experiments H1, H2, and H3.

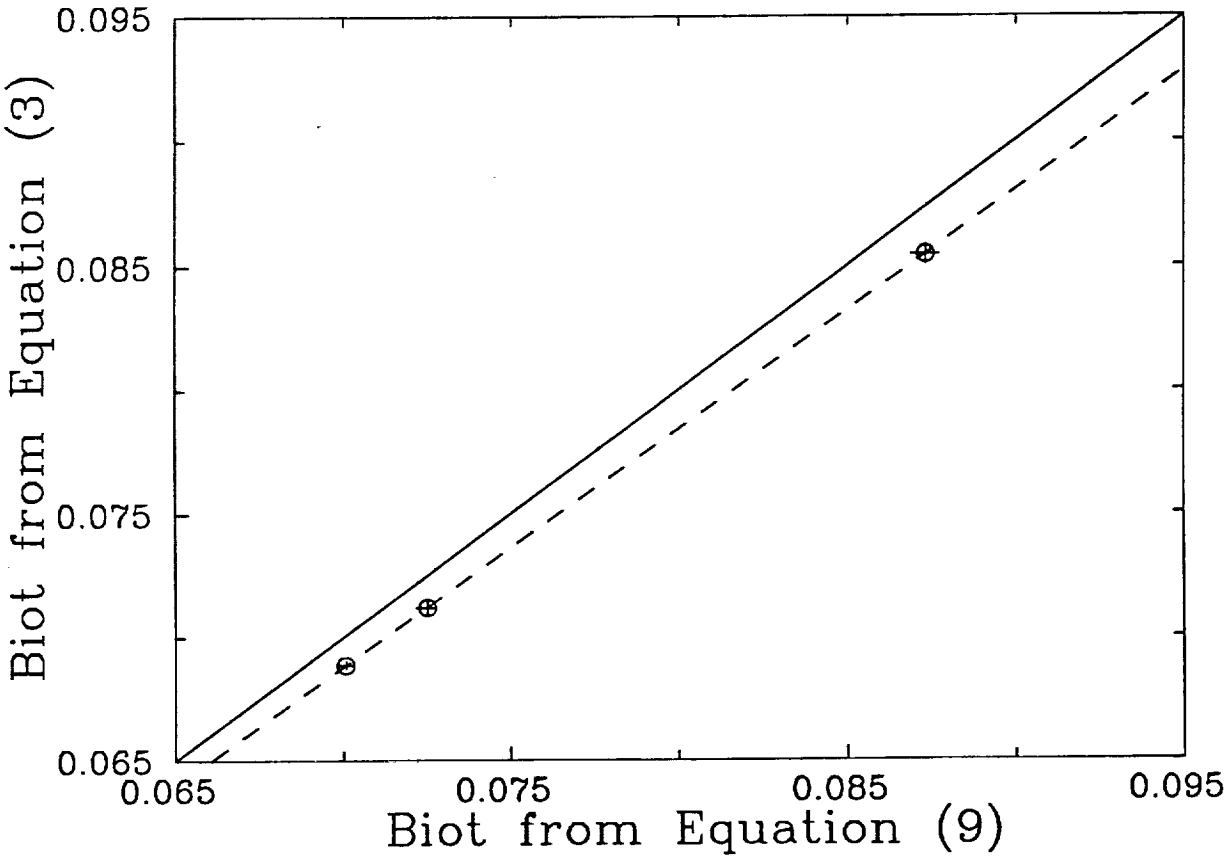

Figure 11. Comparison between the Biot numbers calculated from the slope using equation (3) (lumped-capacity model) and using equation (9). The horizontal and vertical lines in the figure represent 95% confidence limits on the values of the Biot number. The dotted line represents the calculated relative error between the two models and is given by equation (15).